Journal of
Materials Chemistry C

This article can be cited before page numbers have been issued, to do this please use: L. Chen, L. H. Wang and Y. Xiao, *J. Mater. Chem. C*, 2017, DOI: 10.1039/C7TC03171H.

View Article Online
DOI: 10.1039/C7TC03171H

Journal Name

ARTICLE

Heterologous Perylene Diimides Arrays: Potential Non-fullerene Acceptors in Organic Solar Cells

Received 00th January 20xx,
Accepted 00th January 20xx

DOI: 10.1039/x0xx00000x

www.rsc.org/

Helin Wang, Lingcheng Chen* and Yi Xiao*

A new family of perylene diimides (PDI) arrays, heterologous ones (**di-PDI** and **tri-PDI**), were designed and efficiently synthesized by Suzuki cross-coupling reactions using two heterologous PDI monomers at different positions of *bay*- and *ortho*-substitution, respectively. The compounds exhibit unique photophysical and electrochemical properties and were successfully applied in non-fullerene organic solar cells with a superior power conversion efficiency of 4.55% for **tri-PDI**.

1. Introduction

Perylene diimides (PDI) arrays, an important type of PDI derivatives, are constructed by PDI monomers coupling directly through chemical bonds (singly-, doubly-, and triply-linked), no other space linker units.[1] Due to the favorable combined properties of exceptional thermal- and photo-stability, high molar extinction coefficient, and excellent electron-transporting abilities, PDI arrays have been utilized in a variety of applications in organic electronics.[2] Among them, the singly bonded ones have successfully used in organic solar cells (OSCs) as electron acceptors because of their better matching energy levels, flexibility and twisted structures.[3] Especially, through the tailor-made molecular design and synthesis, the singly bonded PDI dimer derivatives have realized great achievement in non-fullerene OSCs, of which the power conversion efficiency (PCE) values are comparable or even superior to those of the corresponding classic fullerene ones.[4] Therefore, the molecular design is a crucial factor affecting the different properties of the materials.

As we know, the PDI monomer contains two different reactive positions: *ortho*- (*α*-) and *bay*- (*β*-) positions (Fig. 1a). Because the *bay* positions of PDI are more reactive toward electrophilic substitutions, *bay*-substituted PDI derivatives have been more highly studied than *ortho*-substituted PDI derivatives.[5, 6] Up to now, all the reported PDI arrays are homologous ones, which are usually synthesized by efficient Ullmann coupling reactions using *bay*-halogenated PDI monomers (Fig. 1b).[7] However, the corresponding heterologous PDI arrays, especially for the ones coupled with *bay*-position and *ortho*-position of the PDI (Fig. 1c), are a great challenge to obtain because of the difficulty of the selective reaction of the *ortho*-positions of PDI. Fortunately, in recent years, the new catalytic systems of Ru- and Ir-based catalysts have been developed to specifically catalyze the *ortho*-positions of PDI, which provides an opportunity to design and synthesize this type of PDI derivatives.[8] In addition, because of the large contribution to the conjugated structures and electron density distributions, substituent effects at the *bay*-positions are substantial, while the substitution at the *ortho*-positions has been proved to be less effective to modify the optical and electronic nature of the parent PDI.[6, 8, 9] Compared to the homologous ones, heterologous PDI arrays maybe own some unique photophysical and electrochemical properties. Inspired by such purpose, we have a desire to achieve this type of heterologous PDI arrays to investigate the intrinsic properties and photovoltaic properties.

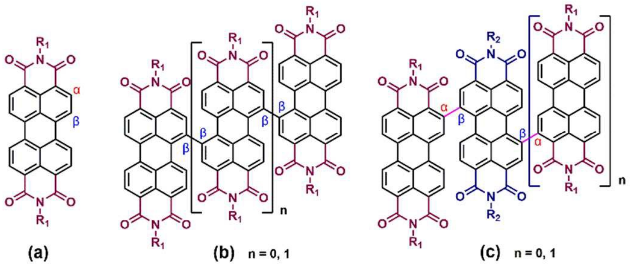

Fig. 1 PDI (a) and their homologous (b), heterologous (c) arrays.

Herein, we present the first examples of the heterologous PDI arrays synthesized by Suzuki cross-coupling reactions with the two heterologous PDI monomers at the *bay*-position and the *ortho*-position, respectively. Their photophysical and electrochemical properties are characterized in details and give some important interesting phenomena. More importantly, these molecules, as non-fullerene electron acceptor materials, have successfully applied in OSCs with the high PCE of 4.55%.

2. Results and discussion

State Key Laboratory of Fine Chemicals, Dalian University of Technology, Dalian, 116024, China. E-mail: lcchen@dlut.edu.cn; xiaoyi@dlut.edu.cn

† Electronic Supplementary Information (ESI) available: [TGA, DFT, UV-vis spectra, OSCs, and NMR]. See DOI: 10.1039/x0xx00000x

View Article Online
DOI: 10.1039/C7TC03171H

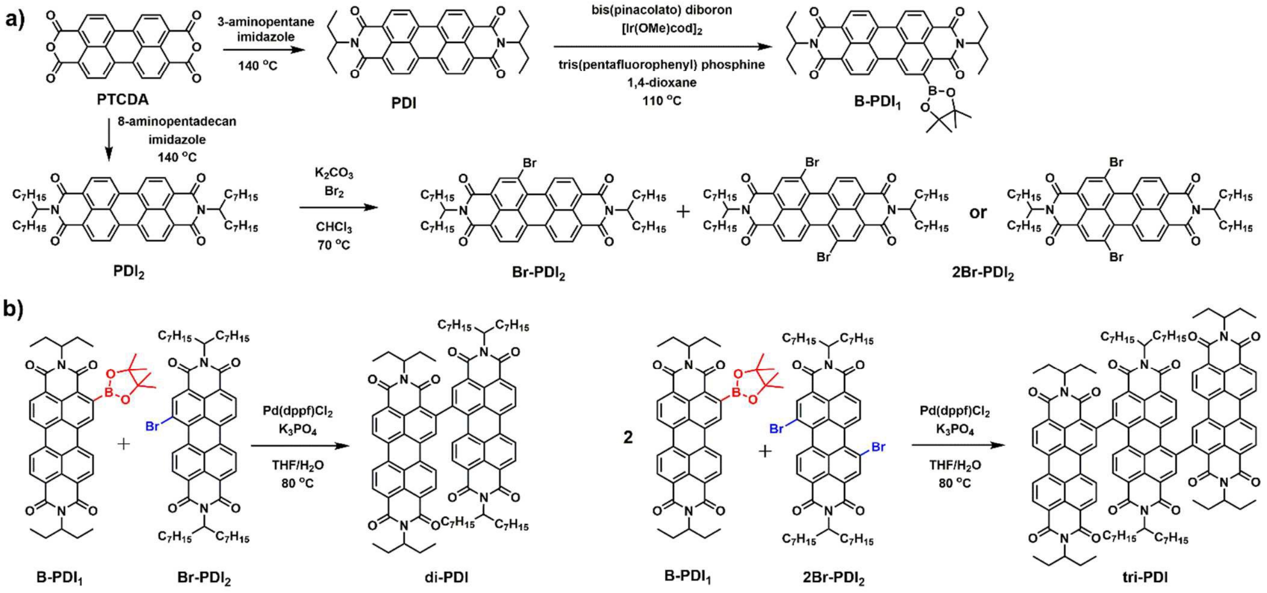

Scheme 1 Synthetic routes of the important intermediates (a) and the target compounds of **di-PDI** and **tri-PDI** (b).

2.1 Synthesis and characterization

Two heterologous PDI molecules (**di-PDI** and **tri-PDI**) were prepared by efficient Suzuki cross-coupling reactions between the *ortho*-position borate of the one PDI and the *bay*-position bromide of the other PDI (Scheme 1) with high yields of 69% and 75% for **di-PDI** and **tri-PDI**, respectively. It should be noted that, the homologous PDI arrays are usually synthesized by the classical Ullmann coupling reactions with the dihalogen- or tetrahalogen-substituted PDI monomers. As a result, a series of homologous PDI arrays with different amount of oligomers are obtained in one-pot synthesis.[7] However, this method is only suitable for the synthesis of homologous PDI arrays, not for the heterologous ones. In addition, it is very difficult to obtain a single PDI array by the column chromatography from the series of oligomers. By contrast, the Suzuki cross-coupling reactions, which were used in our synthesis, are suitable for not only homologous PDI arrays but also heterologous ones. Moreover, the different alkyl or aryl groups connected with imide position of PDI would affect the charge transport, solubility, and the morphology of the thin films, and further determining their optoelectronic properties and device performance.[10] Therefore, we chose two different alkyl-functionalized (3-pentyl for PDI$_1$ and 8-pentadecyl for PDI$_2$) PDI monomers to construct the heterologous PDI arrays. The target compounds **di-PDI** and **tri-PDI** are highly soluble in common organic solvents and fully characterized by ^{1}H-NMR, ^{13}C-NMR spectroscopy and matrix-assisted laser desorption ionization time-of-flight (MALDI-TOF) mass spectrometry. In addition, the compounds exhibit excellent thermal stability with the decomposition temperatures (with 5% weight loss) of 350.1 °C and 383.8 °C for **di-PDI** and **tri-PDI**, respectively (see the ESI†).

2.2 Photophysical properties

As shown in Fig. 2a, three compounds exhibit similar UV-vis absorption spectra in dilute dichloromethane solution and strong absorption with the maximum molar extinction coefficients of 9.0×10^4, 9.0×10^4, and 1.2×10^5 M^{-1}cm^{-1} for N, N'-bis(1-ethylpropyl)perylene-3,4,9,10-tetracarboxylic acid diimides (**PDI**) (Scheme 1), **di-PDI**, and **tri-PDI**, respectively. Compared with that of **PDI** (524 nm), the maximum absorption peaks of **di-PDI** (529 nm) and **tri-PDI** (530 nm) only occur a little red shift with 5 nm and 6 nm because of the enlarged conjugation, which indicate that this method of connection with *ortho*-position and *bay*-position almost retains **PDI**'s inherent absorption property. In thin films (Fig. 2b), every absorption spectra show a relatively broad absorption of 400-600 nm with two peaks at 497 and 538 nm, 498 and 535 nm, 496 and 533 nm for **PDI**, **di-PDI**, and **tri-PDI**, respectively. Although the corresponding maximum peaks in films occur some red shifts relative to those in solution because of the intermolecular interactions, the values of the red shift are becoming small from 14 nm for **PDI** to 3 nm for **tri-PDI**, which reveal that the intermolecular interactions are weakened. More importantly, the ratio of the two maximum peaks have changed a lot, which illustrate that the morphology of molecular aggregation has also changed greatly. In addition, it is important to note that for **PDI**, the maximum absorption in solution is the 0-0 peak, but in the thin film, the maximum absorption is the 0-1 peak because of the very strong intermolecular π-π packing. However, from **di-PDI** to **tri-PDI** in thin film, the peaks of 0-1 gradually weaken while the peaks of 0-0 become more intense, which reveals that the strong intermolecular aggregation has been efficiently inhibited. All these results could be attributed to the reason that the dimer and trimer format the stereo conjugated framework in which the steric hindrance results

View Article Online
DOI: 10.1039/C7TC03171H

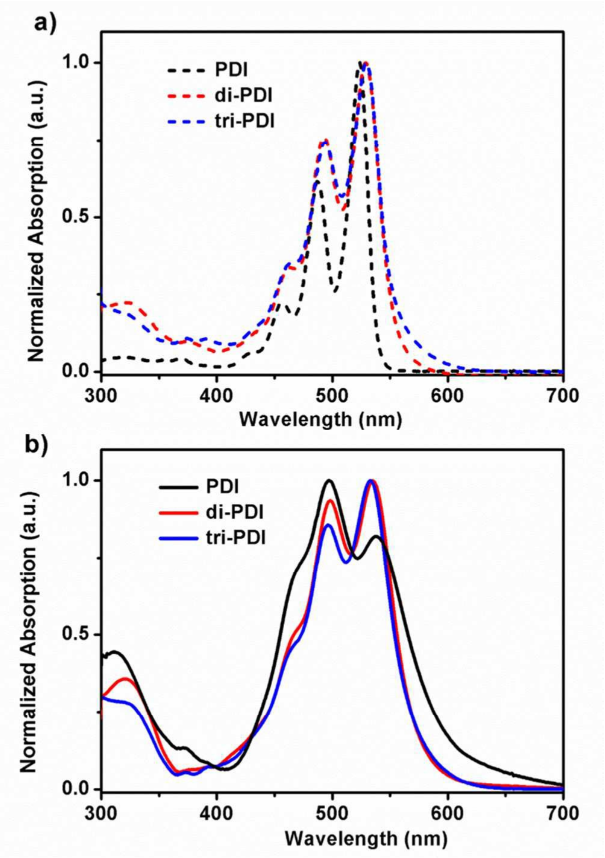

Fig. 2 UV-vis absorption spectra of **PDI**, **di-PDI** and **tri-PDI** in dichloromethane (1×10^{-5}) (a) and in thin films (b).

in non-coplanar structures. As demonstrated by quantum-chemical calculations using density functional theory (DFT) (see the ESI†), there exist big molecular planar distortions of 65° and 75° for **di-PDI** and **tri-PDI**, respectively, between the PDI monomers. All these results indicate that these heterologous PDI arrays could not only retain PDI's unique absorption characteristics, but also prevent the strong intermolecular aggregation.

2.3 Electrochemical properties

The cyclic voltammetry (CV) was employed to investigate their electrochemical properties (Fig. 3a). The compounds **di-PDI** and **tri-PDI** exhibit five and three one-electron reduction waves in dichloromethane, which are more than that of **PDI** with the two reduction waves. With the expansion of π-conjugated system, the first reduction potentials of PDI arrays undergo a positive shift from -1.16 V for **PDI** to -1.07 V for **di-PDI**, and to -1.09 V for **tri-PDI**, indicating the increase of the electron-accepting abilities. From the onset reduction potentials, the lowest unoccupied molecular orbital (LUMO) levels are estimated to be -3.92, -4.01, and -3.99 eV for **PDI**, **di-PDI**, and **tri-PDI**, respectively.

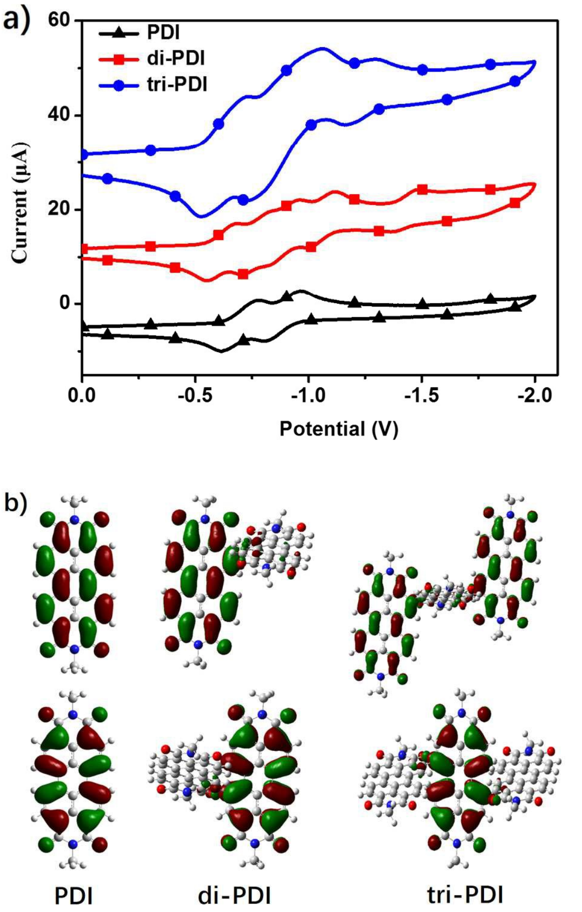

Fig. 3 Cyclic voltammograms of **di-PDI** and **tri-PDI** in DCM (a) and the theoretical calculation of LUMO (upper) and HOMO (blow) electron density distributions with Gaussian DFT-B3LYP/6-31G.

To obtain further insights into the electronic structures of **PDI**, **di-PDI** and **tri-PDI**, their geometries were optimized by DFT calculations at B3LYP/6-31G level. As shown in Fig. 3b, compared to **PDI**, **di-PDI** and **tri-PDI** give the different electron density distributions. What is more interesting is that the LUMO are mainly located on the *ortho*-connected PDI units, while the HOMO are mainly located on the *bay*-connected PDI unit. The asymmetry in the location of the HOMO and LUMO indicates that it is possible for charge transfer to occur from the *ortho*-connected PDI unit to the *bay*-connected PDI unit, while it is not found in the homologous ones.[7d] The calculated LUMO levels of -3.64, -3.85 and -3.84 eV for **PDI**, **di-PDI**, and **tri-PDI**, respectively. Although the calculated LUMO energy levels are slightly higher than those of the observed ones, the regularity of the values is consistent with the experimental data.

2.4 Photovoltaic properties

In order to estimate the photovoltaic properties, using the two PDI derivatives as electron acceptors, non-fullerene OSCs were fabricated with an inverted device architecture of ITO/ZnO/PTB7-Th: **di-PDI** or **tri-PDI** (1:1)/MoO_3/Al, where ITO is indium tin oxide, ZnO and MoO_3 were used as the n and p-type interfacial layers, respectively, to facilitate charge

View Article Online
DOI: 10.1039/C7TC03171H

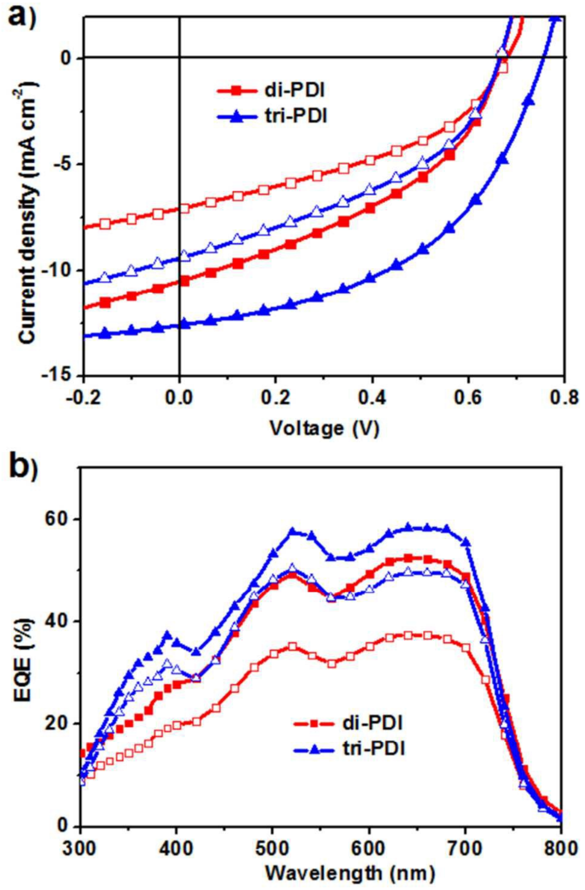

Fig. 4 (a) *J*−*V* curves of the OSCs based on **di-PDI** (red lines) and **tri-PDI** (blue lines) without (open symbols) and with 2% CN (solid symbols) and (b) the corresponding EQE spectra of the devices without (open symbols) and with 2% CN (solid symbols).

transport and collection. PTB7-Th, which has complementary absorption with the electron acceptors (see the ESI†) and well matched energy levels, was chosen as the electron donors. **Fig. 4a** and **Fig. S4-S8** (see the ESI†) show the current density-voltage (*J-V*) curves, and the photovoltaic performance data are listed in **Table 1** and **Table S1-S5** (see the ESI†) for a clear comparison. Firstly, the devices with varying PTB7-Th:**di-PDI** (or **tri-PDI**) mass ratio from 1.5:1 to 1:1.5 were prepared and tested. The device based on PTB7-Th:**tri-PDI** with 1:1 blend ratio shows an optimized average PCE of 2.54% with a J_{SC} of 9.36 mA cm^{-2}, an open circuit voltage (V_{OC}) of 0.661 V, and a fill factor (*FF*) of 41.1%. At the same condition, the other device based on PTB7-Th**:di-PDI** gives a relatively low PCE of 1.95% with a J_{SC} of 7.08mA cm^{-2}, a V_{OC} of 0.673 V, and an *FF* of 40.8%.

Table 1 Photovoltaic properties of the OSCs based on PTB7-Th:**tri-PDI** (or **di-PDI**) = 1:1 under the illumination of AM 1.5G, 100 mW cm^{-2}.

Devices	Add. [vol.]	Temp. [^{o}C]	Jsc [mA cm^{-2}]	Voc [V]	FF [%]	PCE [%]
di-PDI	no	25	7.08	0.673	40.8	1.95
	2% CN	160	10.51	0.661	40.9	2.84
tri-PDI	no	25	9.36	0.661	41.2	2.54
	2% CN	160	12.61	0.751	48.1	4.55

To further enhance the performance of devices, thermal annealing process and some additives such as 1, 8-diodooctane (DIO), chloronaphthalene (CN), and diphenyl ether (DPE) are often used to improve the morphology of the blend films. In our system with the optimal D/A weight ratio of 1:1 (**Table S2 and Fig. S5**) (see the ESI†), when the thermal annealing temperature is 160 °C, the device exhibits the dominant device performance with a PCE of 3.94%. Then when utilizing different amount CN as the additive, all the blend films have obtained the optimal photovoltaic performance, while the PCEs adding DIO and DPE are not improved (**Table S3 and Fig. S6**) (see the ESI†). It is found that the addition of 2% CN can dramatically improve the J_{SC} of devices from 9.36 to 13.41 mA cm^{-2}, accompanied by slight increase of the V_{OC} and *FF* values. Therefore, the device based on PTB7-Th:**tri-PDI** (1:1) with 2% CN additive shows the best performance: J_{SC} of 13.41 mA cm^{-2}, V_{OC} of 0.713 V, *FF* of 40.0%, and PCE of 3.82%. At the same time, the device based on PTB7-Th:**di-PDI** also gives the improved PCE of 2.68% with a J_{SC} of 9.98 mA cm^{-2}, a V_{OC} of 0.661 V, and an *FF* of 40.6% (**Table S4 and Fig. S7**) (see the ESI†). Finally, combined with thermal annealing (160 °C) and the additive of 2% CN (**Fig. 4a** and **Table 1**), the devices exhibit the best photovoltaic performance with a PCE of 4.55%, a J_{SC} of 12.61 mA cm^{-2}, a V_{OC} of 0.751 V, an *FF* of 48.1% and a PCE of 2.84%, a J_{SC} of 10.51 mA cm^{-2}, a V_{OC} of 0.661 V, an *FF* of 40.9% for PTB7-Th:**tri-PDI** and PTB7-Th:**di-PDI**, respectively. In addition, although the homologous PDI trimer array has been synthesized in one-pot synthesis, it is very difficult to obtain a single PDI trimer array by the column chromatography from the series of oligomers and its OSCs device performance was not reported.[7] The detailed comparison of the homologous and heterologous PDI arrays would be a very interesting work to investigate,[11] and the further studies on the comparison are under way and will be presented in a forthcoming paper.

The high J_{SC} values of the devices with 2% CN additive can be confirmed from their external quantum efficiency (EQE) curves of the optimized devices (**Fig. 4b**). The devices show significant photo-to-current responses in the range of 300-800 nm, which agrees well with their absorption spectra of the donor and acceptor materials (**Fig. S3**). After the additive processing, the J_{SC} values are much higher than those of the primitive ones. Especially, for **tri-PDI**-based devices processed with 2% CN, high EQE values over 50% are observed in a wide range of 450-750 nm, with the peak values about 60% at 520 and 630-680 nm. Therefore, **tri-PDI** exhibits the best device performance because of the higher J_{SC} values, which is attributed to the stronger light absorption property. The integrated short circuit current from EQE spectra is consistent with experimental data obtained from the *J*–*V* measurement with a small deviation of less than 5%.

View Article Online
DOI: 10.1039/C7TC03171H

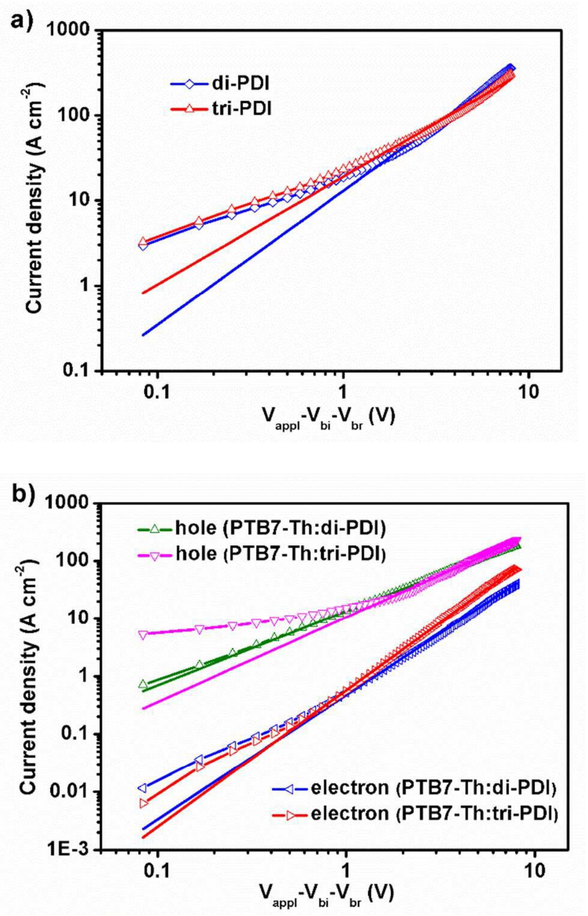

Fig. 5 Current density-voltage curves of the electron- (a, b) and hole-only (b) devices. The lines with symbols are the measured values, and the lines without symbols are the theoretical fitting values.

2.5 Charge Mobilities

To further investigate the relationship of structure-properties-performance of materials, the space-charge-limited current (SCLC) method was used to measure the hole and electron mobilities with the device structures of ITO/PEDOT:PSS/Active layer/MoO_3/Al and ITO/ZnO/Active layer/Ca/Al, respectively.[12] In the pure films (**di-PDI** or **tri-PDI**) SCLC electron-only devices (**Fig. 5a**), **tri-PDI** gives a higher electron mobility of 3.78×10^{-4} $cm^2\ V^{-1}\ s^{-1}$ than that (2.59×10^{-4} $cm^2\ V^{-1}\ s^{-1}$) of **di-PDI**. In their blend film SCLC devices (**Fig. 5b**), the high hole mobilities of 8.39×10^{-5} and 8.69×10^{-5} $cm^2\ V^{-1}\ s^{-1}$ were obtained for PTB7-Th:**di-PDI** and PTB7-Th:**tri-PDI** blend films, respectively. And in their electron-only devices, the relatively low electron mobilities of 1.11×10^{-5} and 1.94×10^{-5} $cm^2\ V^{-1}\ s^{-1}$ were obtained for PTB7-Th:**di-PDI** and **tri-PDI** blend film, respectively. Compared the hole mobilities with the electron ones, the formers are much higher than those of the latter corresponding ones. And the ratio of hole/electron mobilities (μ_h/μ_e) are 7.6 and 4.5 for PTB7-Th:**di-PDI** and PTB7-Th:**tri-PDI** blend film, respectively. Obviously, besides of the higher electron mobility of pure **tri-PDI**, the higher carrier mobilities and more balanced carrier transport of the blend film can partially explain the better solar cell performance observed in the **tri-PDI** OSCs than those of the **di-PDI** ones.

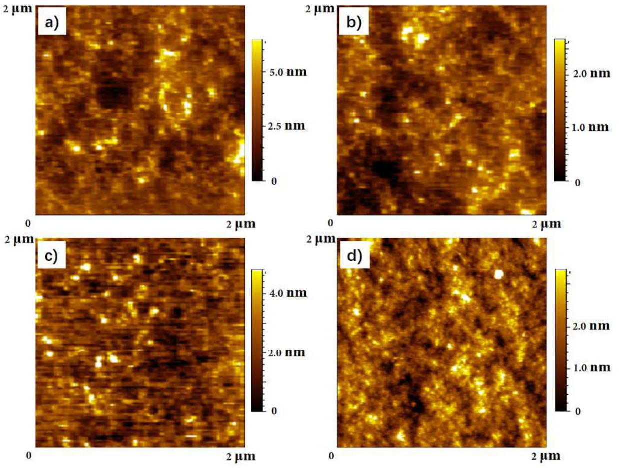

Fig. 6 AFM height images of the active layers based on PTB7-Th:**di-PDI** blend without (a) and with (c) 2% CN additive, PTB7-Th:**tri-PDI** blend without (b) and with (d) 2% CN additive.

2.6 Active layer morphology

The nanoscale phase-separation morphology also plays an important role on the performance of the OSC devices. As shown in **Fig. 6**, the blend films without treatment based on PTB7-Th:**di-PDI** and PTB7-Th:**tri-PDI** both show large-size phase- separated domains, and the root-mean-square (RMS) roughness are 14.4 and 10.3 nm, respectively. After the optimization of thermal annealing and additive processing, the surface of the blend films becomes smoother with the RMS of 6.1 and 3.2 nm for PTB7-Th:**di-PDI** and PTB7-Th:**tri-PDI** blends, respectively. Especially, the surface of PTB7-Th:**tri-PDI** blends gives the favorable morphology and small-size phase separation, which are in accordance with the much better performance of the PTB7-Th:**tri-PDI** device.

3. Conclusions

In summary, a new family of PDI arrays, heterologous PDI oligomers, were designed and synthesized through efficient Suzuki cross-coupling reactions between the *ortho*-position borate of the one PDI monomer and the *bay*-position bromide of the other PDI monomer. The absorption spectra revealed that the two compounds not only retain the prototype **PDI**'s intrinsic characteristics of strong absorption in visible light region, but also could prevent the strong intermolecular aggregation in thin films due to the stereo conjugated molecular configurations. In electrochemical characterization, **di-PDI** and **tri-PDI** exhibited more negative LUMO levels of about -4.0 eV, which are slightly lower than that of **PDI**. A very interesting result is that, for the heterologous PDI arrays, there may be existing intramolecular charge transfer from one PDI to the other PDI unit. Used the two compounds as electron acceptors, the non-fullerene OSCs device based on **tri-PDI** gave a superior performance up to 4.55%. All these results indicate

View Article Online
DOI: 10.1039/C7TC03171H

that developing heterologous PDI derivatives have provided the other way to investigate the non-fullerene electron acceptors for high efficiency OSCs.

4. Experimental section

Materials and General Methods

All reagents were purchased from Aldrich or Acros and used without further purification. Solvents for chemical synthesis were purified according to the standard procedures. All chemical reactions were carried out under an inert atmosphere. The indium-tin oxide (ITO) on glass was purchased from Xiangcheng Science and Technology Co. Ltd. All chemical reactions were carried out under an inert atmosphere.

^{1}H and ^{13}C NMR spectra were recorded using a 500 MHz Bruker in $CDCl_3$ at 293 K using TMS as a reference. Accurate mass correction were measured with matrix-assisted laser desorption-ionization time-of-flight (MALDI-TOF) mass spectrometer (MALDI micro MX). UV-vis spectra were measured with UV-vis spectrophotometer (Model HP8453) in a 1 cm quartz cell. Cyclic voltammograms (CVs) were recorded on a BSA100B/W electrochemical workstation using glassy carbon discs as the working electrode, Pt wire as the counter electrode, Hg/Hg_2Cl_2 electrode as the reference electrode at a scanning rate of 0.1 V/s. 0.05 M tetrabutylammoniumhexafluorophosphate (Bu_4NPF_6) dissolved in dichloromethane was employed as the supporting electrolyte, which was calibrated by the ferrocene/ferroncenium (Fc/Fc^+) as the redox couple. The energy of Fc/Fc^+ is 5.08 eV relative to vacuum.[13] Thermogravimetric Analysis (TGA) were carried out using a Mettler Toledo TGA/SDTA 851e at a heating rate of 10 ^{o}C min^{-1} under nitrogen flow of 20 mL min^{-1}.

Geometry optimizations were optimized by the density functional theory (DFT) at the B3LYP/6-31G level. All the calculations were performed using the Gaussian 09 program. To simplify the calculation, alkyl chains were replaced by CH_3 groups. AFM measurements were performed in a tapping mode. All film samples were spincasted on ITO/ZnO substrates with the same conditions of the corresponding OSC devices.

OSC Devices Fabrication and Measurements

The ITO glass plates were cleaned in a sonication bath in acetone, isopropyl alcohol and deionized water sequentially, dried by blowing nitrogen, and then treated with O_2 plasma for 15 min before use. About 25 nm thick ITO-modifying layer of ZnO was spin-coated on top of ITO and then baked for 30 min at 200 °C. Then the PTB7-Th and **di-PDI** (or **tri-PDI**) blend liquid was spin-coated on the ZnO layer to get an 80 nm thick film. Finally, MoO_3 and Al layers were evaporated on top of the active layer. The device area, the overlap section between the ITO and Al electrodes, was about 7 mm^2.

The photocurrent–voltage (*J-V*) characteristics of the solar cells were measured using a Keithley 2400 Source-measure unit under illumination of a simulated sunlight (AM 1.5G, 100mW· cm^{-2}) provided by an Oriel Sol3A solar simulator (Newport USA, Model: 94023A) with an AM 1.5 filter in ambient air. The IPCE characterization of all devices was performed in ambient air by a Hypermono-light (SM-25, Jasco Co. Ltd., Japan). A calibrated Si photodiode (818-UV Newport) was used as a reference in order to determine the intensity of the light incident on the device, allowing the IPCE spectrum to be deduced.

SCLC Devices fabrication and testing

The ITO glass plates with 15 Ω cm^{-2} resistor were cleaned in a sonication bath in acetone, isopropyl alcohol and deionized water sequentially, dried by blowing nitrogen, and then treated with O_2 plasma for 15 min before use. For the electron-only devices: a thin layer (~25 nm) of ZnO sol-gel was spin-coated at 4,000 rpm. for 40 seconds onto ITO glasses and annealed at 200 ^{o}C in ambient condition for one hour then transferred into glove box immediately. Active layers were spin-coated using the prepared solutions at 1000 rpm. for 30 seconds in a glove box, and the thickness is about 300 nm. After that, the substrate was transferred to a vacuum thermal evaporator, followed by deposition of the Ca/Al (10 nm/100 nm) cathode at a base pressure of 4×10^{-4} Pa. And for the hole-only devices: a thin layer (~45 nm) of PEDOT:PSS was spin-coated at 4,000 rpm. for 40 seconds onto ITO glasses and annealed at 120 ^{o}C in ambient condition for 30 min. then transferred into glove box. Active layers were spin-coated using the prepared solutions at 1000 rpm. for 30 seconds in a glove box, and the thickness is about 300 nm. After that, the substrate was transferred to a vacuum thermal evaporator, followed by deposition of the MoO_3/Al (10 nm/100 nm) cathode at a base pressure of 4×10^{-4} Pa. All SCLC devices were characterized with a computer-controlled Keithley 2420 source measure unit.

Synthesis

PTB7-Th is purchased from Solarmer Materials Inc., while other commercially available reagents were purchased from Sigma Aldrich, Alfa Aesar Co., TCI chemical Co., Thermo Fisher Scientific Inc. and used without further purification unless otherwise stated. Considering the mixture of **2Br-PDI$_2$**, the target molecule **tri-PDI** is also a mixture. In order to the facilitation of the discussion, we use the one structure to instead.

Compound **N,N'-Bis(1-ethylpropyl)perylene-3,4,9,10-tetracarboxylic acid bisimide** (**PDI**): A mixture of 3,4,9,10-Perylenetetracarboxylic acid dianhydride (1 g, 2.55 mmol), 3-aminopentane (0.75 mL, 6.44 mmol) and imidazole (10 g, 0.15 mol) was stirred under nitrogen at 140 ^{o}C for 4 hours. After that, water was added and the mixture was extracted with dichloromethane. The organic layers were washed with brine and dried over $MgSO_4$. The solvent was removed under reduced pressure, and the residue was purified by silica gel column chromatography with dichloromethane as eluent. Compound **PDI** was obtained in 90 % yield (1.2 g, 2.26 mmol).^{1}H NMR (500 MHz, $CDCl_3$, 25 ^{o}C): δ (ppm) = 8.82-8.67 (m, 4H), 8.60-8.57 (d, 2H), 8.56-8.55 (d, 2H), 5.09-5.03 (m, 2H), 2.23-2.19 (m, 4H), 1.96-1.91 (m, 4H), 0.93-0.91 (t, 12H).

View Article Online
DOI: 10.1039/C7TC03171H

Compound **N,N'-Bis(1-ethylpropyl)-2-(4,4,5,5-tetramethyl-1,3,2-dioxaborolan-2-yl)- perylene-3,4,9,10-tetracarboxylic acid bisimide** (**B-PDI$_1$**)[14]: A mixture of **PDI** (1 g, 1.89 mmol), bis (pinacolato) diboron (0.75 g, 2.95 mmol), $[Ir(OMe)cod]_2$ (38 mg, 0.06 mmol) and tris (pentafluorophenyl) phosphine (120 mg, 0.24 mmol) in 5 mL of 1,4-dioxane was stirred under nitrogen at 110 °C for 48 hours. The solvent was removed under reduced pressure, and the residue was purified by silica gel column chromatography with dichloromethane as eluent. Compound **B-PDI$_1$** was obtained in 45 % yield (0.56 g, 0.85 mmol). ^{1}H NMR (500 MHz, $CDCl_3$, 25 °C) : δ (ppm) = 8.67-8.65 (d, 1H), 8.58-8.56 (d, 3H), 8.54-8.51 (m, 2H), 8.46 (s, 1H), 5.09-4.97 (m, 2H), 2.28-2.23 (m, 4H), 1.97-1.95 (m, 4H), 1.58 (s, 12H), 0.94-0.92 (t, 12H); MALDI-TOF-MS: Calcd for $C_{40}H_{41}BN_2O_6$, 656.3058 [M$^-$], found 656.3006.

Compound **N,N'-Bis(1-heptyloctyl)perylene-3,4,9,10-tetracarboxylic acid diimide** (**PDI$_2$**): A mixture of 3,4,9,10-Perylenetetracarboxylic acid dianhydride (1 g, 2.55 mmol), 8-aminopentadecan (1.28 g, 5.63 mmol) and imidazole (15 g, 0.23 mol) was stirred under nitrogen at 140 °C for 5 hours. After that, water was added and the mixture was extracted with dichloromethane. The organic layers were washed with brine and dried over $MgSO_4$. The solvent was removed under reduced pressure, and the residue was purified by silica gel column chromatography with petroleum ether:dichloromethane =1:1 as eluent. Compound **PDI$_2$** was obtained in 93 % yield (1.92 g, 2.37 mmol). ^{1}H NMR (500 MHz, $CDCl_3$, 25 °C) : δ (ppm) =8.96-8.78 (m, 4H), 8.64-8.62 (d, 2H), 8.56- 8.54 (d, 2H), 5.16-5.14 (m, 2H), 2.24-2.22 (m, 4H), 1.84-1.81 (m,4H), 1.60-1.10 (m, 40H), 0.92-0.88 (m, 12H).

Compound **N,N'-Bis(1-heptyloctyl)-1-bromo-perylene-3,4,9,10-tetracarboxylic acid diimide** (**Br-PDI$_2$**) and **N,N'-Bis(1-heptyloctyl)-1,6-bibromo-perylene-3,4,9,10- tetracarboxylic acid diimide** and **N,N'-Bis(1-heptyloctyl)-1,7-bibromo-perylene- 3,4,9,10-tetracarboxylic acid diimide** (**2Br-PDI$_2$**): A mixture of **PDI$_2$** (1 g, 1.23 mmol), anhydrous potassium carbonate (3.4 g, 24.64 mmol) and bromine (5 mL, 0.1 mol) in chloroform (20 mL) was stirred at 70 °C for 8 hours. The excess bromine was removed by adding aqueous Na_2SO_3. Water was added and the mixture was extracted with chloroform. The organic layers were washed with brine and dried over $MgSO_4$. The solvent was removed under reduced pressure, and the residue was purified by silica gel column chromatography with petroleum ether:dichloromethane =3:2 as eluent. Compound **Br-PDI$_2$** was obtained in 41 % yield (0.41 g, 0.46 mmol), ^{1}H NMR (500 MHz, $CDCl_3$, 25 °C) : δ (ppm) =9.79 (d, 1H), 8.92-8.70 (m, 4H), 8.62 (d, 2H), 5.17-5.15 (m, 2H), 2.26-2.22 (m, 4H), 1.85-1.81 (m,4H), 1.60-1.10 (m, 40H), 0.91-0.88 (m, 12H). Compound **2Br-PDI$_2$** were obtained in 46 % yield (0.55 g, 0.57 mmol), ^{1}H NMR (500 MHz, $CDCl_3$, 25 °C) : δ (ppm) =9.49 (d, 2H), 8.90 (d, 2H), 8.65-8.58 (m, 2H), 5.17-5.14 (m, 2H), 2.23-2.21 (m, 4H), 1.85-1.81 (m,4H), 1.60-1.10 (m, 40H), 0.92-0.88 (m, 12H).

Compound **di-PDI**: A mixture of **B-PDI$_1$** (0.2 g, 0.31 mmol), and **Br-PDI$_2$** (0.3 g, 0.34 mmol), $Pd(dppf)Cl_2$ (30 mg, 0.04 mmol) and 1 M aqueous potassium phosphate (2 mL) in THF (10 mL) was stirred at 80 °C for 8 hours. After that, water was added and the mixture was extracted with chloroform. The organic layers were washed with brine and dried over $MgSO_4$. The solvent was removed under reduced pressure, and the residue was purified by silica gel column chromatography with petroleum ether:dichloromethane =1:10 as eluent. Compound **di-PDI** was obtained in 69 % yield (0.28 g, 0.21 mmol). ^{1}H NMR (500 MHz, $CDCl_3$, 25 °C) : δ (ppm) = 8.86-8.85 (d, 1H), 8.80-8.78 (d, 1H), 8.77-8.70 (m, 6H), 8.54-8.51 (d, 2H), 8.42-8.40 (d, 2H), 8.01-7.97 (d, 1H), 7.83-7.80 (d, 1H), 5.19-4.77 (m, 4H), 2.28-2.01 (m, 8H), 1.95-1.74 (m, 8H), 1.25-1.22 (m, 40H), 0.90-0.83 (m, 24H); ^{13}C NMR (125 MHz, $CDCl_3$, 25 °C) : δ (ppm) = 164.77, 163.74, 163.39, 163.37, 147.98, 143.32, 141.37, 136.12, 134.82, 134.27, 133.50, 131.58, 131.08, 129.58, 129.32, 128.98, 128.80, 128.55, 128.40, 127.93, 127.28, 126.48, 126.44, 125.37, 123.72, 123.66, 122.97, 57.87, 57.80, 54.84, 54.66, 31.81, 31.73, 29.54, 29.42, 29.24, 29.23, 29.14, 27.00, 26.88, 22.62, 22.55, 14.06, 14.01, 11.29; MALDI-TOF-MS: Calcd for $C_{88}H_{98}N_4O_8$, 1338.7385 [M$^-$], found 1338.7363.

Compound **tri-PDI**: A mixture of **2Br-PDI$_2$** (0.12 g, 0.13 mmol), and **B-PDI$_1$** (0.2 g, 0.31 mmol), $Pd(dppf)Cl_2$ (23 mg, 0.03 mmol) and 1 M aqueous potassium phosphate (2 mL) in THF (10 mL) was stirred at 80 °C for 8 hours. After that, water was added and the mixture was extracted with chloroform. The organic layers were washed with brine and dried over $MgSO_4$. The solvent was removed under reduced pressure, and the residue was purified by silica gel column chromatography with petroleum ether:dichloromethane =1:9 as eluent. Compound **tri-PDI** was obtained in 75 % yield (0.17 g, 0.091 mmol). ^{1}H NMR (500 MHz, $CDCl_3$, 25 °C): δ (ppm) = 8.86-8.76 (m, 8H), 8.65-8.59 (m, 8H), 8.06-8.01 (m, 2H), 7.84-7.77 (m, 2H), 5.11-5.07 (m, 4H), 5.06-4.78 (m, 2H), 2.29-2.25 (m, 8H), 1.97-1.92 (m, 8H), 1.76-1.73 (m, 8H), 1.25-1.18 (m, 40H), 0.95-0.77 (m, 36H); ^{13}C NMR (125 MHz, $CDCl_3$, 25 °C) : δ (ppm)= 164.48, 163.38, 147.17, 140.71, 136.15, 135.92, 134.92, 134.68, 134.37, 134.23, 133.65, 133.40, 132.75, 132.36, 130.93, 129.63, 129.58, 128.88, 128.42, 128.30, 126.54, 126.47, 125.97, 124.05, 123.63, 120.63, 57.78, 54.72, 32.35, 32.21, 31.75, 29.70, 29.46, 29.16, 26.89, 25.02, 24.85, 24.61, 22.57, 14.04, 11.32, 11.13, 10.98; MALDI-TOF-MS: Calcd for $C_{122}H_{126}N_6O_{12}$, 1866.9434 [M$^-$], found 1866.9447.

Acknowledgements

This work is supported by National Natural Science Foundation of China (Nos. 21376038, 21421005, 21406027, and 21576040), National Basic Research Program of China (No. 2013CB733702), Dalian Agency for Science and Technology (No. 2015R040), and the Fundamental Research Funds for the Central Universities (No. DUT16RC(4)02).

Notes and references

View Article Online
DOI: 10.1039/C7TC03171H

1 (a) C. Li and H. Wonneberger, *Adv. Mater.*, 2012, **24**, 613-636; (b) W. Jiang, Y. Li and Z. H. Wang, *Acc. Chem. Res.*, 2014, **47**, 3135-3147.

2 (a) A. F. Lv, S. R. Puniredd, J. H. Zhang, Z. B. Li, H. F. Zhu, W. Jiang, H. L. Dong, Y. D. He, L. Jiang, Y. Li, W. Pisula, Q. Meng, W. P. Hu and Z. H. Wang, *Adv. Mater.*, 2012, **24**, 2626-2630; (b) J. H. Zhang, L. Tan, W. Jiang, W. P. Hu and Z. H. Wang, *J. Mater. Chem. C*, 2013, **1**, 3200-3206; (c) W. Jiang, L. Ye, X. G. Li, C. Y. Xiao, F. Tan, W. C. Zhao, J. H. Hou and Z. H. Wang, *Chem. Commun.*, 2014, **50**, 1024-1026.

3 (a) L. Ye, W. Jiang, W. C. Zhao, S. Q. Zhang, D. P. Qian, Z. H. Wang and J. H. Hou, *Small*, 2014, **10**, 4658-4663; (b) Y. Zang, C. Z. Li, C. C. Chueh, S. T. Williams, W. Jiang, Z. H. Wang, J. S. Yu and A. K. Y. Jen, *Adv. Mater.*, 2014, **26**, 5708-5714.

4 (a) D. Sun, D. Meng, Y. H. Cai, B. B. Fan, Y. Li, W. Jiang, L. J. Huo, Y. M. Sun and Z. H. Wang, *J. Am. Chem. Soc.*, 2015, **137**, 11156-11162; (b) A. D. Hendsbee, J. P. Sun, W. K. Law, H. Yan, I. G. Hill, D. M. Spasyuk and G. C. Welch, *Chem. Mater.*, 2016, **28**, 7098-7109; (c) D. Meng, D. Sun, C. M. Zhong, T. Liu, B. B. Fan, L. J. Huo, Y. Li, W. Jiang, H. Choi, T. Kim, J. Y. Kim, Y. M. Sun, Z. H. Wang and A. J. Heeger, *J. Am. Chem. Soc.*, 2016, **138**, 375-380.

5 (a) X. W. Zhan, Z. A. Tan, B. Domercq, Z. An, X. Zhang, S. Barlow, Y. F. Li, D. B. Zhu, B. Kippelen and S. R. Marder, *J. Am. Chem. Soc.*, 2007, **129**, 7246-7247; (b) Y. Z. Lin, Y. F. Wang, J. Y. Wang, J. H. Hou, Y. F. Li, D. B. Zhu and X. W. Zhan, *Adv. Mater.*, 2014, **26**, 5137-5142; (c) H. L. Zhong, C. H. Wu, C. Z. Li, J. Carpenter, C. C. Chueh, J. Y. Chen, H. Ade and A. K. Y. Jen, *Adv. Mater.*, 2016, **28**, 951-958; (d) Y. K. Guo, Y. K. Li, O. Awartani, J. B. Zhao, H. Han, H. Ade, D. H. Zhao and H. Yan, *Adv. Mater.*, 2016, **28**, 8483-8489; (e) D. Meng, H. T. Fu, C. Y. Xiao, X. Y. Meng, T. Winands, W. Ma, W. Wei, B. B. Fan, L. J. Huo, N. L. Doltsinis, Y. Li, Y. M. Sun and Z. H. Wang, *J. Am. Chem. Soc.*, 2016, **138**, 10184-10190; (f) S. X. Li, W. Q. Liu, C. Z. Li, T. K. Lau, X. H. Lu, M. M. Shi and H. Z. Chen, *J. Mater. Chem. A*, 2016, **4**, 14983-14987; (g) Y. Zhong, M. T. Trinh, R. S. Chen, G. E. Purdum, P. P. Khlyabich, M. Sezen, S. Oh, H. M. Zhu, B. Fowler, B. Y. Zhang, W. Wang, C. Y. Nam, M. Y. Sfeir, C. T. Black, M. L. Steigerwald, Y. L. Loo, F. Ng, X. Y. Zhu and C. Nuckolls, *Nat. Commun.*, 2015, **6,** 8242-8247.

6 (a) D. L. Zhao, Q. H. Wu, Z. X. Cai, T. Y. Zheng, W. Chen, J. Lu and L. P. Yu, *Chem. Mater.*, 2016, **28**, 1139-1146; (b) Q. H. Wu, D. L. Zhao, A. M. Schneider, W. Chen and L. P. Yu, *J. Am. Chem. Soc.*, 2016, **138**, 7248-7251.

7 (a) H. L. Qian, Z. H. Wang, W. Yue and D. B. Zhu, *J. Am. Chem. Soc.*, 2007, **129**, 10664-10665; (b) H. L. Qian, F. Negri, C. R. Wang and Z. H. Wang, *J. Am. Chem. Soc.*, 2008, **130**, 17970-17976; (c) Y. G. Zhen, C. R. Wang and Z. H. Wang, *Chem. Commun.*, 2010, **46**, 1926-1928; (d) W. Jiang, C. Y. Xiao, L. X. Hao, Z. H. Wang, H. Ceymann, C. Lambert, S. D. Motta and F. Negri, *Chem. Eur. J.*, 2012, **18**, 6764-6775.

8 (a) S. Nakazono, S. Easwaramoorthi, D. H. Kim, H. Shinokubo and A. Osuka, *Org. Lett.*, 2009, **11**, 5426-5429; (b) S. akazono, Y. Imazaki, H. Yoo, J. Yang, T. Sasamori, N. Tokitoh, T. Cédric, H. Kageyama, D. Kim, H. Shinokubo and A. Osuka, *Chem. Eur. J.*, 2009, **15**, 7530-7533; (c) G. Battagliarin, C. Li, V. Enkelmann and K. Müllen, *Org. Lett.*, 2011, **13**, 3012-3015.

9 P. E. Hartnett, A. Timalsina, H. S. S. R. Matte, N. J. Zhou, X. G. Guo, W. Zhao, A. Facchetti, R. P. H. Chang, M. C. Hersam, M. R. Wasielewski and T. J. Marks, *J. Am. Chem. Soc.*, 2014, **136**, 16345-16356.

10 P. E. Hartnett, E. A. Margulies, H. S. S. R. Matte, M. C. Hersam, T. J. Marks and M. R. Wasielewski, *Chem. Mater.*, 2016, **28**, 3928-3936.

11 H. Yin, Y. Geng, G. Y. Sun and Z. M. Su, *J. Phys. Chem. C*, 2017, **121**, 2125-2134.

12 P. N. Murgatroyd, *J. Phys. D: Appl. Phys.,* 1970, **3**, 151-156.

13 B. C. Thompson, Y.-G. Kim, T. D. McCarley and J. R. Reynolds, *J. Am. Chem. Soc.,* 2006, **128**, 12714-12725.

14 T. Teraoka, S. Hiroto and H. Shinokubo, *Org. Lett.,* 2011, **13**, 2532-2535.

View Article Online
DOI: 10.1039/C7TC03171H

TOC

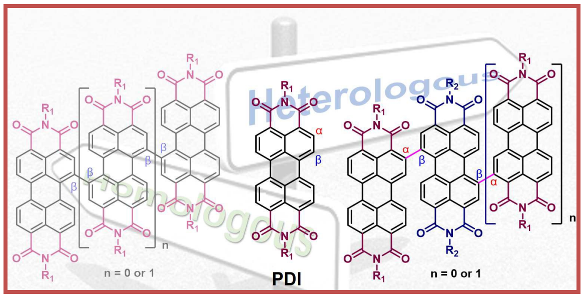

A new family of perylene diimides (PDI) arrays, heterologous ones, were efficiently developed for non-fullerene organic solar cells with a superior PCE of 4.55%.